Ultrafast photoelectron spectroscopy of aqueous solutions

Cite as: J. Chem. Phys. **151**, 090901 (2019); https://doi.org/10.1063/1.5098402
Submitted: 02 April 2019 . Accepted: 14 May 2019 . Published Online: 03 September 2019

Toshinori Suzuki

J. Chem. Phys. **151**, 090901 (2019); https://doi.org/10.1063/1.5098402 **151**, 090901

The Journal of Chemical Physics | PERSPECTIVE | scitation.org/journal/jcp

Ultrafast photoelectron spectroscopy of aqueous solutions

Cite as: J. Chem. Phys. 151, 090901 (2019); doi: 10.1063/1.5098402
Submitted: 2 April 2019 • Accepted: 14 May 2019 •
Published Online: 3 September 2019

Toshinori Suzuki[a)]

AFFILIATIONS

Department of Chemistry, Graduate School of Science, Kyoto University, Kitashirakawa-Oiwakecho,
Sakyo-Ku, Kyoto 606-8502, Japan

[a)]**Email:** suzuki.toshinori.2n@kyoto-u.ac.jp

ABSTRACT

Chemical reaction dynamics in liquids and at interfaces are central themes in the materials, energy, and environmental sciences. Ultrafast photoelectron spectroscopy of liquids enables unprecedented access to the electronic dynamics of transient chemical species, providing deeper insights into nonadiabatic reaction dynamics in aqueous solutions, which are strongly coupled with solvation dynamics.

I. INTRODUCTION

The 1974 paper by Smalley *et al.* demonstrated that the highly congested electronic spectrum of NO_2 at room temperature is drastically simplified by adiabatic cooling in a supersonic jet expansion.[1] Later, a combination of molecular beam techniques and laser mass spectrometry led them to the celebrated discovery of C_{60}.[2] Similarly, the successful marriage of molecular beam methods and laser spectroscopy in the past four decades resulted in a number of breakthroughs in gas-phase studies of molecular structures and reaction dynamics. Ultrafast spectroscopy has captured the decisive moments of chemical reactions at the transition state and at the conical intersection of potential energy surfaces,[3] and crossed molecular beam scattering with laser-spectroscopic detection of products enabled clear identification of quantum mechanical (Feshbach) resonances[4] in elementary bimolecular reactions.[5–7] These studies have now extended to research in attosecond electron dynamics,[8] cold molecular collisions,[9] and many other new frontiers. Remarkable progress has also been made in theoretical and computational studies with the advent of computers and sophisticated approximation methods.[10,11] The accuracy of electronic structure calculations has reached a spectroscopic level, and accurate quantum wave packet[12] and molecular dynamics simulations of large molecular systems have become possible.[13,14] Now, steps must be taken to elucidate the reaction dynamics in more complex systems.

From this point of view, aqueous solutions are one of the most important targets of research, as they are central in the biological, materials, environmental, and energy sciences. Water is indispensable for life,[15] and it is also the most intriguing liquid[16,17] because it acts as both a proton donor and acceptor, significantly alters the electronic energy of a solute through electrostatic interactions, and exhibits structural order/disorder dynamics in its hydrogen bonding network. Water is not a mere solvent but a crucial player in aqueous chemistry.

Since molecular reaction dynamics is primarily driven by electrons, deep understanding of (transient) electronic states is the key for elucidating reaction mechanisms. Photoelectron spectroscopy[18] is a powerful experimental method to probe the electronic structure of matter, as it enables the direct measurement of an electron binding energy (eBE).[19–22] Pioneering efforts to use photoelectron spectroscopy for the elucidation of electronic structures of liquids have been made by Delahay,[23] Siegbahn,[24] and others in late 1960s–1970s.[25] Delahay sampled a thin liquid layer on the surface of a rotating disk and photoexcited it with monochromatized vacuum UV (VUV) radiation to determine the photoemission threshold energy.[23,26] They also measured the photoelectron kinetic energy (PKE) distribution at a given photon energy using a variable retardation potential. Hans Siegbahn and co-workers[24] tried a number of novel methods, such as using a rotating wetted wire, to introduce a liquid sample into an X-ray photoelectron spectrometer under high vacuum.[27] Morgner and co-workers reported a detailed study on the depth profile of hydrophobic tetrabutylammonium cations in formamide using their original liquid-flowing device.[28] In 1973, Siegbahn and Siegbahn reported XPS using a liquid beam with a

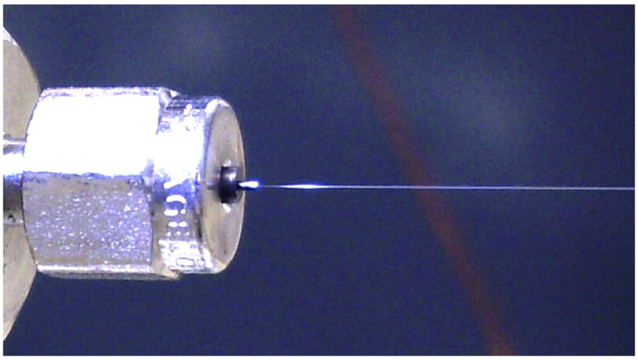

FIG. 1. Liquid microjet discharged from a fused silica capillary. The capillary is a standard tube with a 25-μm inner diameter used for gas chromatography.

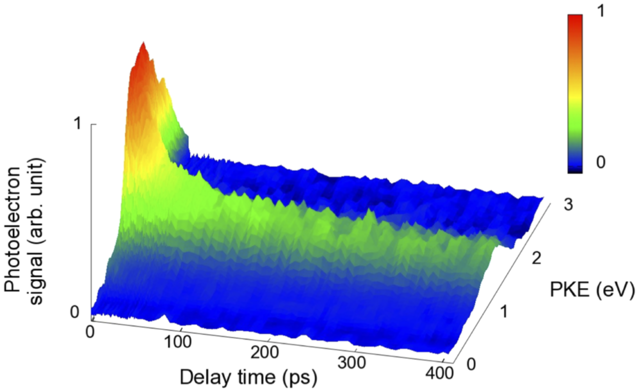

FIG. 2. Photoelectron kinetic energy distribution measured as a function of pump-probe delay time for an aqueous 0.14 mol/l NaI solution. The pump and probe laser wavelengths are 243 and 260 nm, respectively. Reproduced with permission from Tang *et al.*, Phys. Chem. Chem. Phys. **12**, 3653 (2010). Copyright 2010 PCCP Owner Societies.

diameter of about 0.2 mm, which was applicable to a sample with a vapor pressure of less than 1 Torr.[29] In the 1980s, Faubel generated a liquid microjet[30] with a diameter of about 10 μm by discharging a pressurized liquid through a pinhole (later a fused silica capillary was introduced as a liquid-discharging nozzle).[31] The microjet (Fig. 1) enabled the introduction of volatile liquids into photoelectron spectrometers because the small surface area of a microjet minimizes solvent evaporation. Its high traveling speed (>10 m/s) enables rapid transport prior to spontaneous freezing by evaporative cooling and continuous replacement of the sample against radiation damage. Using microjets, Faubel *et al.* performed He(I) photoelectron spectroscopy of liquids,[32] while Kondow and co-workers reported photoionization mass spectrometry.[33–35] Despite the great efforts of these pioneers, technical difficulties and the lack of suitable light sources hampered the development of photoelectron spectroscopy of liquids. However, Winter and Faubel implemented liquid microjets for XPS at Berlin electron-storage ring or Berliner Elektronenspeicherring-Gesellschaft für Synchrotronstrahlung, m.b.h. (BESSY), taking advantage of its intense and tunable X-ray radiation from the third generation synchrotron radiation facility, and made great progress in this field.[36] Today, many synchrotron radiation facilities have beamlines that enable XPS of liquid microjets.

Static photoelectron spectroscopy offers valuable information on the electronic structure of liquids, while ultrafast photoelectron spectroscopy is necessary for the real-time observation of electron transfer and redox reactions to capture the time-evolution of the population and eBEs of transient chemical species. In this perspective, we offer a brief overview of the current status of ultrafast photoelectron spectroscopy of aqueous solutions.[37–45]

II. FIRST ULTRAFAST PHOTOELECTRON SPECTROSCOPY: HYDRATED ELECTRON

The first ultrafast photoelectron spectroscopy of aqueous solution was reported in 2010 by several workers[37–39] on the hydrated electron (e^-_{aq}). The hydrated electron is similar to a well-known solvated electron in liquid ammonia,[46] and it was identified for the first time by Hart and Boag in 1962 using pulse radiolysis of liquid water.[47] This transient species is also created in a living cell by irradiation.[48] The hydrated electron is the simplest reducing agent in aqueous chemistry. While its reducing power depends critically on its eBE, the value was not known for a long time. From extrapolation of the values for negatively charged water clusters, Coe *et al.* predicted the vertical eBE (VBE: the energy required to remove an electron without a change in nuclear geometry) of e^-_{aq} in bulk water to be 3.3 eV.[49–51] Neumark and co-workers identified three isomers for water cluster anions, and they concluded that the cluster series I, analyzed by Coe *et al.*, holds an electron internally;[52] the other series were speculated to bind an excess electron on the surface.[52,53] Turi and co-workers refuted this speculation, claiming that all of these water cluster anions bind an excess electron on the cluster surface.[46,54,55] If so, extrapolation of the cluster values will not provide a correct prediction of the bulk value. The ultrafast photoelectron spectroscopy in 2010 sought to solve this problem by measuring the eBE of e^-_{aq} in bulk solution. Figure 2 is the result reported by Tang *et al.*, who photoexcited a charge-transfer-to-solvent (CTTS) band[57,58] of I^- in aqueous NaI solution and measured photoelectron spectra as a function of pump-probe time delay.[38,59] With increasing delay time, the width of the observed PKE distribution rapidly narrowed and the intensity gradually decreased. The VBE after several 100 ps was 3.3 eV, which was attributed to thermally relaxed e^-_{aq}. The conclusion was essentially correct; however, all experimental reports in 2010[37–39,56] are now known to have contained inaccuracies, and the current best estimate of eBE of e^-_{aq} is 3.76 eV.[60] In Sec. III, we examine the fundamentals of ultrafast photoelectron spectroscopy of liquids.

III. EXPERIMENTAL METHODOLOGY

A. Liquid microjet photoelectron spectrometer

A typical photoelectron spectrometer for liquids is illustrated in Fig. 3. A liquid is pressurized with an HPLC (high-pressure liquid chromatography) pump and discharged from a fused silica capillary

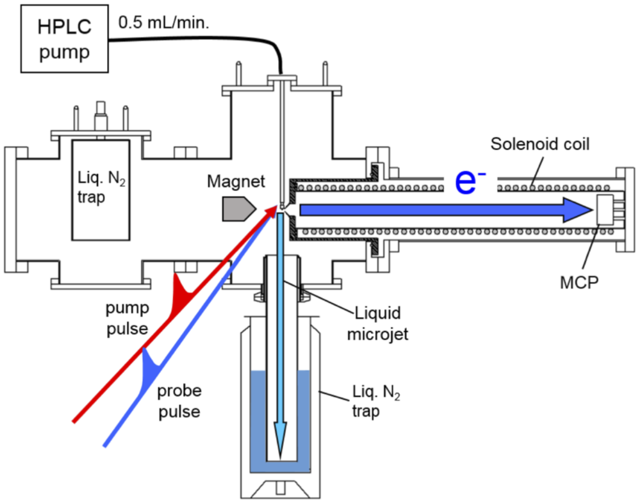

FIG. 3. Schematic diagram of a magnetic bottle time-of-flight photoelectron spectrometer using a liquid microjet. HPLC: high-pressure liquid chromatography and MCP: microchannel plate. Vacuum pumps are not indicated in the figure for simplicity.

15–25 μm in inner diameter. After intersecting with laser beams, the microjet is frozen in a beam catcher maintained at liquid nitrogen temperature. (Alternatively, one can collect the jet into a beam catcher at room temperature through an extremely small entrance hole to recycle it for subsequent measurements.) A typical liquid flow rate is 0.5 ml/min. Pump and probe laser pulses illuminate the microjet at about 1 mm downstream from the nozzle. Photoelectrons emitted from the liquid surface are sampled through a skimmer with an opening diameter of 0.1–2 mm, which facilitates differential pumping of a photoionization chamber and an electron energy analyzer. A strong permanent magnet and a solenoid coil guide more than 50% of the photoelectrons emitted from the liquid to the detector.[61] The electrons are detected using a microchannel plate at the end of a flight tube, and the signal is averaged using a multichannel scaler. Based on the flight time from the sample to the detector, the photoelectron speed and PKE are calculated. Compared with a hemispherical electron energy analyzer,[59] a TOF spectrometer is advantageous in that it enables the measurement of the entire PKE distribution on a shot-to-shot basis and significantly improves the efficiency and reliability of measurements. A typical UV light source is a 1-kHz Ti:sapphire amplifier and optical parametric amplifiers, which enable the generation of tunable radiation from the infrared to deep UV. EUV light is created using cascaded four wave mixing in filamentation[62–64] or high harmonic generation (HHG).[65,66]

An (near) ambient pressure photoelectron spectrometer (APPS) is a new type of instrument that enables the observation of photoelectron spectra at higher pressures (<1 Torr).[67–69] The instrument utilizes multistage differential pumping of an electrostatic lens system placed in front of a hemispherical electrostatic electron energy analyzer. The APPS is mainly employed in XPS for *in situ* (*operando*) observation of catalytic reactions on a solid surface exposed to gases, while Artiglia *et al.* demonstrated the studies on heterogeneous reactions at liquid-gas interfaces using a liquid microjet and a gas dosing system.[70] As far as we noticed, the APPS has not yet been employed for ultrafast photoelectron spectroscopy of liquids; however, its excellent differential pumping capability will certainly be useful for ultrafast photoelectron spectroscopy of liquid microjets, liquid sheets, and droplet trains.

B. Light source

Photoelectron spectroscopy requires that the photon energy be greater than the eBE of the material being investigated. Therefore, photons in the region from the UV to X-ray are needed. Among various light sources, synchrotron radiation facilities provide by far the best performance in this energy region in terms of their wide wavelength coverage, high photon flux, and simultaneous photon supplies to numerous beamlines. Since space-charge effects (Coulombic repulsion among photoelectrons) must be avoided in photoelectron spectroscopy, the number of photoelectrons generated per pulse should be minimized. Consequently, a small electron count per pulse must be compensated by a high repetition rate of the light source. Synchrotron radiation is typically operated at about 100 MHz, and its photon flux is unrivaled. However, the typical pulse duration of synchrotron radiation is on the order of tens of picoseconds, so it is not ideal for ultrafast spectroscopy. Free electron lasers (FELs)[71] have drastically improved the performance of ultrafast spectroscopy in the X-ray region with their significantly shorter pulse duration and higher pulse energy. However, the main disadvantage of the FELs in operation thus far is that their repetition rates are 60–120 Hz. New FEL facilities providing kilohertz to megahertz repetition rates will lead to breakthroughs in ultrafast X-ray spectroscopy.

HHG is currently one of the best methods for generating femtosecond EUV pulses for ultrafast photoelectron spectroscopy of liquids.[65,66] In HHG, the strong electric field of an intense laser pulse distorts the Coulombic potential of a noble gas to induce tunneling ionization, and a liberated photoelectron accelerated in the oscillating electric field of the laser pulse coherently recombines with an ion to create a burst of electromagnetic waves. This radiation consists of odd-order harmonics of the driving laser frequency due to symmetry conservation. In standard ultrafast photoelectron spectroscopy of liquids with femtosecond time resolution, both time and energy structures of a photoelectron signal are analyzed. Therefore, a single-order harmonic must be isolated from the series of odd-order harmonics to ensure sufficient energy resolution. Time-preserving and time-compensating monochromators using a grating in the off-plane mount are specially designed to provide sufficient spectral resolution to separate harmonics with minimum pulse stretching.[72,73] A much simpler setup for isolating a single harmonic is the use of multilayer mirrors;[74] however, these mirrors are available only for the selected wavelength regions and their rejection of the neighboring orders is imperfect (the reflectivity of the neighboring order radiation is roughly 10% of that for the main order at each mirror). A zone plate has also been employed in some applications.[75]

HHG is possible using well-established 1 kHz Ti:sapphire amplifiers; however, it is desirable to drive HHG at much higher repetition rates for photoelectron spectroscopy. As an example, Corder *et al.* constructed a cavity-enhanced HHG light source using an 88-MHz 1.03-μm Yb-based frequency comb, as shown in Fig. 4.[76] The photon flux at 25.1 eV was estimated to be

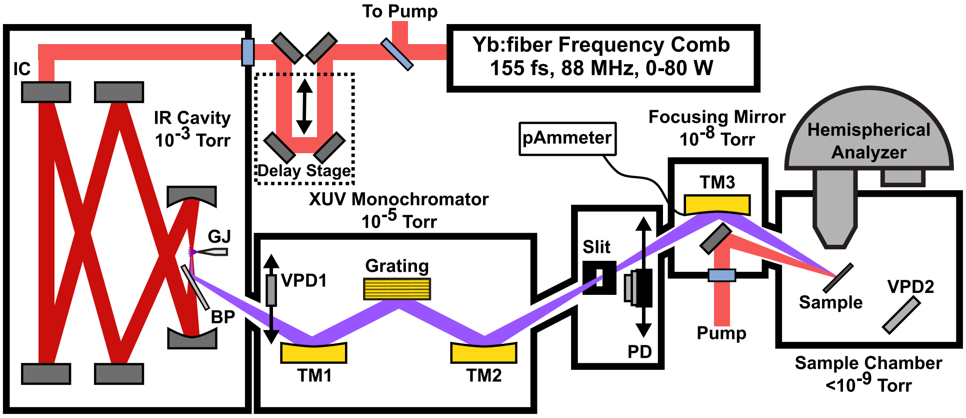

FIG. 4. Cavity-enhanced HHG source and photoelectron spectrometer. High-order harmonics of a resonantly enhanced Yb:fiber frequency comb are generated at the focus of a six-mirror enhancement cavity and coupled into an XUV beamline. A pulse-preserving monochromator selects one harmonic, which is focused on a sample under UHV conditions. BP = Brewster plate, VPD = vacuum photodiode, TM = toroidal mirror, PD = XUV photodiode, GJ = gas jet, and IC = input coupler. Reproduced with permission from Corder *et al.*, Struct. Dyn. **5**, 054301 (2018). Copyright 2018 Author(s), licensed under a Creative Commons Attribution 4.0 (CC-BY) License.

7×10^{11} photons/s. Similarly, HHG using fiber lasers[77,78] or thin-disk lasers[79,80] operated at megahertz repetition rates have been reported. Since one-color photoelectron spectroscopy only requires a photon flux, these high repetition rate lasers are very useful. In contrast, pump-probe photoelectron spectroscopy measures an enhanced signal with a good signal-to-noise ratio against the one-color background, for which laser systems with the repetition rate of 0.1–1 MHz might be more suitable to maintain reasonably high pulse energies.

The density of a solute in a typical aqueous solution is more than two orders of magnitude smaller than that of the solvent molecules. Since the photoexcitation efficiency of a solute is several percent in the perturbation regime, the signal from transient species will be 4–6 orders of magnitude smaller than that from the solvent. For detecting such a small signal, it is essential to completely isolate a single order harmonic of radiation; the other harmonics cause background signals. With a single off-plane-mount grating, it is difficult to reduce the neighboring orders to less than 0.1% relative to the harmonic of interest using an 800-nm driving laser. A shorter driving laser wavelength enables superior isolation of a single order, since adjacent HHG orders are separated by twice the driving laser photon energy. Although a shorter wavelength driving laser has a smaller pulse energy, it is compensated in part by the enhanced HHG efficiency owing to smaller quantum diffusion (spatial broadening of a photoelectron wave packet upon coherent recombination with a noble gas ion).[81–83] In most cases, noble gases are used as nonlinear media for HHG. Although HHG in solids has been investigated recently, the aim of such research is to study electron dynamics in solids and to alter the polarization of high harmonics[84–88] rather than to develop an intense EUV light source. An interesting attempt is to use liquids as nonlinear media because liquids provide comparable material density with solids as well as continuous replacement through their flow. Wörner and coworkers have recently demonstrated HHG using water, methanol, and ethanol to produce radiation with a photon energy of less than 20 eV.[89]

C. Electrokinetic charging

One of the problems of a liquid microjet is that it is spontaneously charged.[32,90–92] This phenomenon, known as electrokinetic charging, must be considered in photoelectron spectroscopy of liquid microjets for the accurate determination of eBE. Faubel *et al.* reported that electrokinetic charging can be reduced by increasing the conductivity of a liquid through the addition of an electrolyte or shifting the pH.[32,90] Preissler *et al.*[93] and Kurahashi *et al.*[94] showed that the electric potential of a microjet of aqueous NaX (X: halogen) solution discharged from a fused-silica capillary reverses its polarity at a particular electrolyte concentration, indicating that charging can be avoided by adjusting the NaX concentration. The zero-crossing point was found near 30 mM for an aqueous NaX solution at a flow rate of 0.5 ml/min.[94] That is why 0.03–0.1 mol/l NaCl was added to aqueous solutions of DNA bases to perform its photoelectron spectroscopy, even if the concentrations of the bases were 1–5 mmol/l.[95–97] The mechanism of electrokinetic charging and its electrolyte concentration dependence are not fully understood, but it is related to the acid-base equilibria at the silica surface.[98] The silanol group on the silica surface is negatively charged except at very low pH,[99–104] and adsorption of singly charged Na^+ is not expected to reverse the net surface charge; Kurahashi *et al.* suggested that the observed reversal of the liquid surface potential is related to the adsorption of Na^+ to a siloxane bond (Si–O–Si) on the silica surface at high NaX concentrations.[98]

If the electrokinetic charging is stable, it is not problematic for EUV/X-ray photoelectron spectroscopy, because all electrons emitted from the liquid are equally influenced by the electric potential, and this energy-shift can be evaluated using the eBE (11.3 eV) of solvent water as an internal energy standard.[94,105,106] On the other hand, UV photoelectron spectroscopy of aqueous solutions requires a more elaborate energy calibration using a reference gas, since liquid water is not ionized by UV radiation.[94,107] The electric potential of a liquid microjet can be varied to a desirable value by applying an electric potential to a liquid-discharging nozzle (and liquid), which is useful for differentiating photoelectron signals from the microjet and evaporated gases.

D. Electron scattering in liquid

Photoemission from liquids consists of three steps: (1) promotion of an electron into the conduction band of the liquid, (2) electron transport in the conduction band, and (3) transmission through the liquid-gas interface. During step (2), an electron undergoes elastic, vibrational-inelastic, and electronic-inelastic scattering with solvent molecules. Inelastic scattering at electron kinetic energy higher than 100 eV is dominated by electronic inelastic scattering with an energy loss of greater than 1 eV. In this region, scattering efficiency is expressed by the inelastic mean free path (IMFP),[108] which varies with kinetic energy in an inverse-bell-shaped curve whose minimum lies at 50–100 eV for almost all materials; this characteristic energy dependence of the IMFP is referred to as "a universal curve" (Fig. 5). Since the IMFP increases monotonically beyond 100 eV, HAXPES (hard X-ray photoelectron spectroscopy) gains a high bulk sensitivity. According to the universal curve,[109] one may anticipate that the probing depth of photoelectron spectroscopy increases very rapidly as the electron kinetic energy decreases below 50 eV; however, this is not the case. Elastic scattering cross sections are quite large in the low kinetic energy region, causing zig-zag electron trajectories and increasing the number of scattering events. Under such conditions, scattering efficiency is more properly expressed using an effective attenuation length (EAL). It is the length over which an electron flux diminishes by a factor of 1/*e*.

There have been only a few studies to estimate the EAL in liquid water using photoelectron spectroscopy of microjets. Winter and co-workers attempted this using O(1s) photoemission intensity of liquid water as a function of electron kinetic energy from 50 to 900 eV.[110] After measuring the O(1s) intensity, they calibrated the absolute length scale of EAL using photoemission intensities of Na^+ and I^- measured for aqueous NaI solution under similar experimental conditions. The calibration led to large ambiguities, however, because it employed theoretically predicted depth profiles of Na^+ and I^- in an aqueous solution, estimated photoemission cross sections, and assumed photoemission anisotropy of O(1s).[110] The last factor was experimentally measured in their later study, and it reduced the estimation of EAL values to smaller than 1 nm in the kinetic energy region below 100 eV.[111] Suzuki and co-workers compared O(1s) photoemission intensity from a liquid water microjet and water vapor around the jet to estimate the absolute length scale of the EAL in liquid water.[112] The EALs they estimated were slightly greater than the theoretical predictions in the energy region above 100 eV, while it remained as 1–2 nm in the kinetic energy region below 100 eV. Shinotsuka *et al.* compared the IMFP in liquid water calculated from the optical energy-loss function using various theoretical models.[113] Different theoretical methods provide very similar IMFP values for energies over 300 eV, while the values largely differ in the region less than 100 eV. More recently, Nguyen-Truong improved the Mermin-Penn algorithm to calculate electron scattering at low kinetic energy and obtained better agreement with experimental values; the calculated IMFP was 1–3 nm for 10–100 eV.[114] Signorell and co-workers carried out photoelectron imaging of neutral water clusters (or nanodroplets) and analyzed electron scattering using Monte-Carlo simulations with their own estimates of cross sections.[115,116] White and co-workers estimated the EAL in amorphous ice on Pt(111) to be 0.87 nm at 0.35 eV,[117] while Kurtz *et al.* reported >1.3 nm at 18 eV for amorphous ice on Cu(100).[118] Sanche and co-workers[48] performed a low-energy electron backscattering experiment from amorphous solid ice at 14 K, an example of which is shown in Fig. 6. Inelastic scattering in ice at low kinetic energy is mainly due to the vibrational excitations of intermolecular translational (25 meV) and librational (62–95 meV) modes and intramolecular bending (205 meV) and stretching (422–460 meV) modes.[119] The electronic inelastic scattering starts in the kinetic energy around 7.5 eV. Shinotsuka *et al.* suggested that the relatively large IMFP obtained by Sanche and colleagues can be ascribed to the porous structure,[113] while Nguyen-Truong speculates that the IMFP is longer in ice than in liquid water due to the higher structural order and smaller mass density.[114]

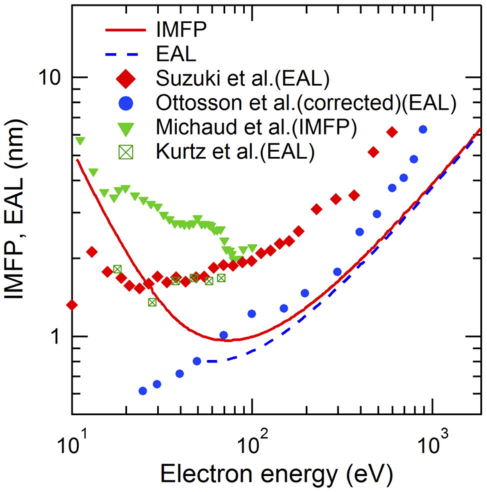

FIG. 5. Experimentally measured EALs and IMFPs for liquid water and ice; Suzuki *et al.*[112] (solid diamonds), Ottosson *et al.*[110] (solid circles) as corrected by Thürmer *et al*,[111] Kurtz *et al.*[118] (half-solid squares), and IMFP from Michaud *et al.*[120] (downward triangles). The solid and dashed lines show calculated IMFPs and EALs, respectively. Adapted with permission from Shinotsuka *et al.*, Surf. Interface Anal. **49**, 238 (2017). Copyright 2017 Author(s), licensed under a Creative Commons Attribution 4.0 (CC-BY) License.

It would be fair to conclude that theoretical estimations of IMFP and EAL in liquid water are not highly reliable for the kinetic energy region below 100 eV, and experimental investigations in this region are not sufficiently accurate either. Both theoretical and experimental investigations are further needed to solve this fundamental problem.

In EUV and X-ray photoelectron spectroscopy, the PKE distribution generally exhibits sharp spectral features due to unscattered electrons and a broad background from scattered and/or secondary electrons. In UV photoelectron spectroscopy, the distributions of unscattered and scattered electrons overlap so that spectral analysis becomes complicated. The blurring of UV photoelectron spectra has been observed by Delahay and co-workers in their pioneering experiments; they found that the PKE distribution of a glycerol solution of $Li_3[Fe(CN)_6]$ exhibited increasing spectral broadening with higher UV photon energy.[121] They concluded that the electron escape depth increases with the photon energy and that a greater

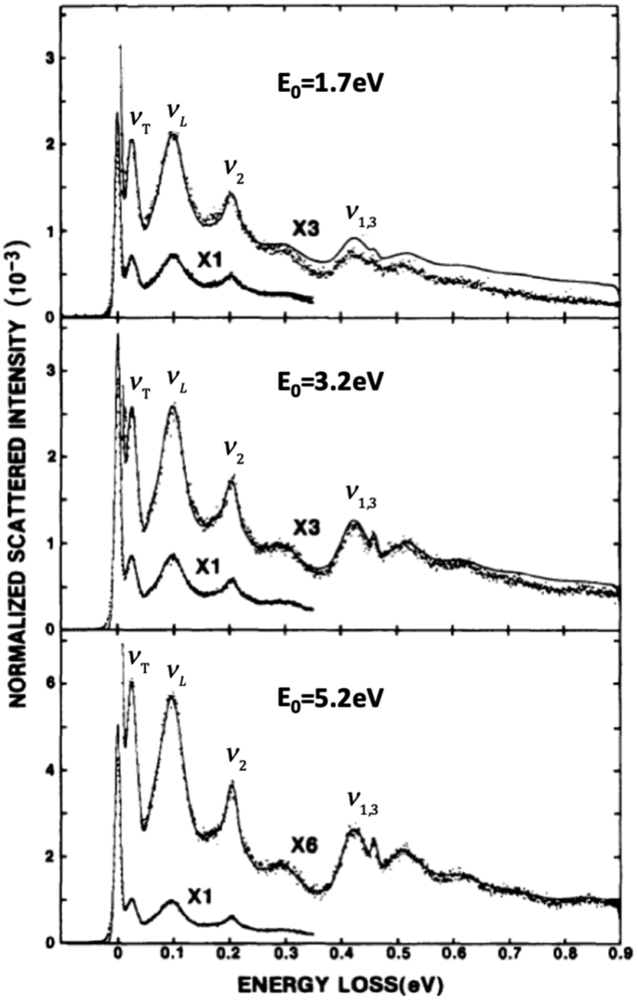

FIG. 6. Electron energy-loss spectra of 30-layer ice films for various incident energies. The dotted curves represent the normalized energy-loss spectra at an incident angle θ_o = 14° and an analysis angle θ_d = 45°. The superimposed solid curves are the calculated energy distributions of backscattered electrons resulting from a two-stream analysis of the spectra. Adapted with permission from M. Michaud and L. Sanche, Phys. Rev. A **36**, 4684 (1987). Copyright 1987 American Physical Society.

number of inelastically scattered electrons contribute to the spectrum.[122] As they increased the photon energy to 21.2 eV, the distributions of unscattered and scattered electrons were separated.[123] In Sec. IV A, we will see how a spectral retrieval method helps overcome this obstacle in UV photoelectron spectroscopy.[60]

The final step in photoemission process is electron transmission through the liquid-gas interface. Quantum mechanical scattering of a particle at the boundary is determined by its kinetic energy and the potential energy gap, so the electron transmission depends on the energy difference (V_0) between the conduction band minimum and the vacuum level; V_0 is essentially an electron affinity of a liquid. The V_0 value of liquid water has not yet been established. In 1997, Bernas, Ferradini, and Jay-Gerin suggested a V_0 value for liquid water of 0.75 V.[124] Coe suggested a smaller value close to zero, 0.2 to −0.3 eV. A recent computational study by Gaiduk *et al.* obtained a V_0 for liquid water of 0.2 eV,[125] while Ambrosio *et al.* (0.8 eV)[126] and Ziaei and Bredow (1.1 eV)[127] claimed larger values. The influence of electron transmission at the interface is well recognized in photoelectron spectroscopy as the cut-off function; however, its rigorous functional form has not been established. In EUV photoelectron spectroscopy, the influence of a cut-off function is negligible, as the PKEs are far greater than V_0. A simple argument based on classical mechanics and an isotropic photoelectron angular distribution provides the following expression for transmission efficiency $T(E)$:

$$T(E) = 1 - \sqrt{\frac{V_0}{E + V_0}}.$$

E. Pump-probe space charge effect

When photoelectrons are generated in high densities, Coulombic repulsion between them alters their kinetic energies, causing broadening and shifting of the distribution. This is a well-known space charge effect, and the number of electrons generated per laser pulse should be minimized to avoid it. In addition to this effect, which occurs under a single laser pulse, a more complex space charge effect occurs in pump-probe photoelectron spectroscopy, in which the electron packet produced by one-color photoemission with the pump pulse repels the electron packet subsequently produced by two-color photoemission induced with the probe pulse. Oloff *et al.* observed the pump-probe space charge effect in their laser-pump and XFEL-probe experiment of solid targets, and they modeled it using a mean field approximation.[128] The model assumes that the pump pulse creates a disk-shaped uniform electron density moving away from the solid surface, and an electron generated by the probe pulse experiences repulsion from the pump packet. Later, Al-Obaidi *et al.* reported a similar problem in UV-EUV ultrafast photoelectron spectroscopy of liquids, in which they took into account the positive charges on the liquid surface created by the pump pulse.[129] The mean field model works reasonably well for calibrating the experimental result against pump-probe space charge effects.[130]

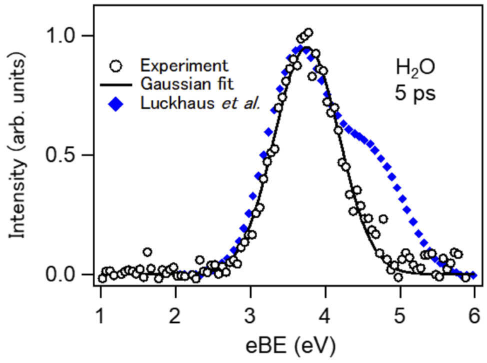

FIG. 7. Photoelectron spectrum of e^-_{aq} in aqueous 0.5 mol/l NaI solution generated using 240-nm excitation of the CTTS (Charge Transfer to Solvent) band of I⁻ and photoemission at 44.4-nm at a delay time of 5 ps. Blue diamonds indicate prediction by Luckhaus *et al.*[60]

IV. RECENT STUDIES

A. Spectral retrieval method in UV photoelectron spectroscopy

The VBE of e^-_{aq} measured using photoelectron spectroscopy of liquid microjets[37–39,56] was in fair agreement with the prediction by Coe *et al.*[49] However, Yamamoto *et al.* showed that these experimental estimates of VBE were possibly inaccurate because inelastic scattering in the liquid alters the electron kinetic energy in the conduction band prior to emission from the liquid-gas interface.[131] Luckhaus *et al.* performed Monte-Carlo simulations of electron scattering in liquid water that took into account energy-dependent differential cross sections of elastic and inelastic scattering of an electron in liquid water, and they retrieved what was considered to be the genuine eBE distribution.[60] The analysis indicated that VBE is best estimated to be 3.7 eV. Interestingly, the eBE distribution exhibited a shoulder on the high eBE side.

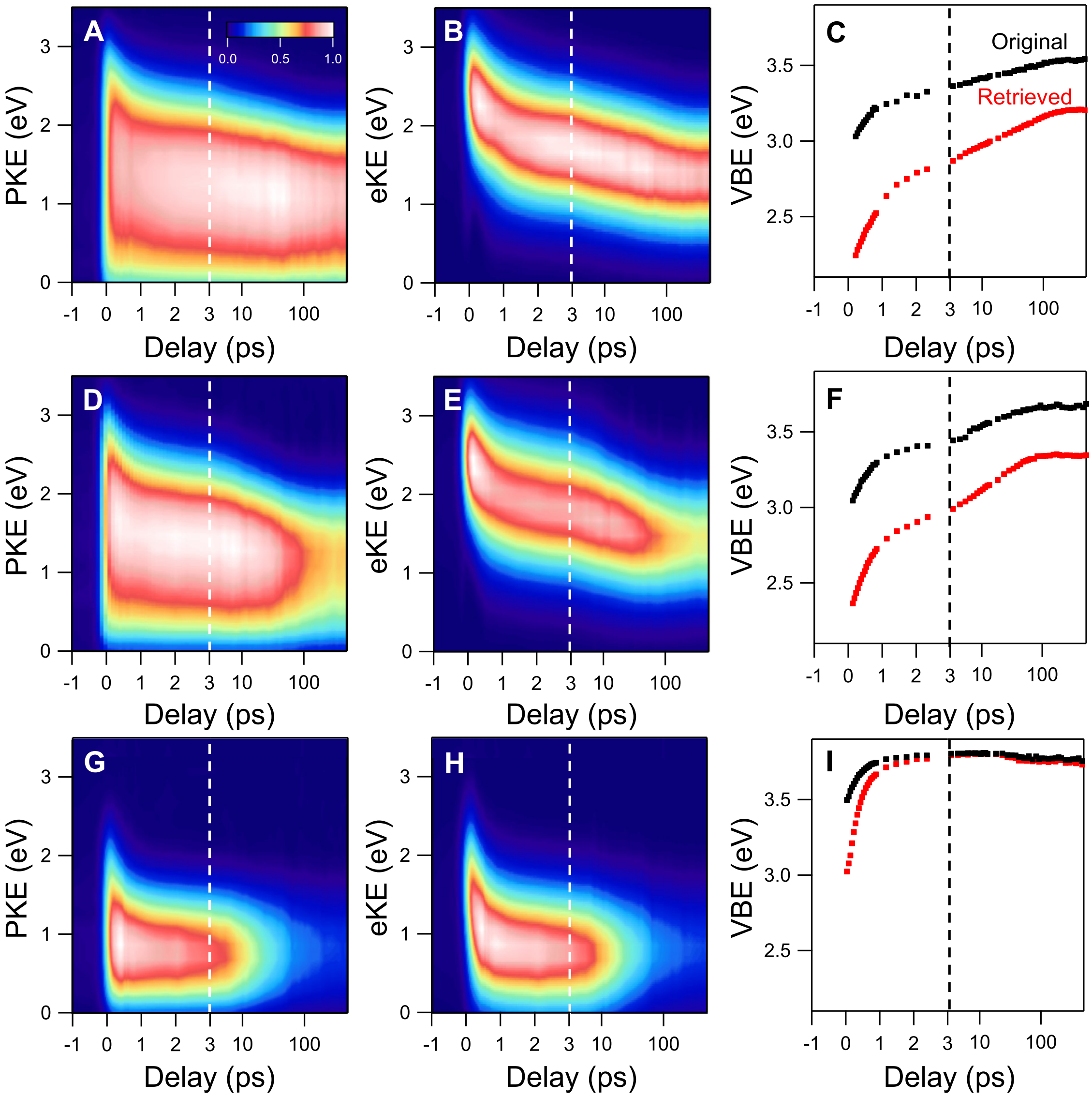

FIG. 8. Ultrafast UV photoelectron spectra of the CTTS reaction from I$^-$ to polar protic solvents. PKE time-energy map measured for (a) ethanol, (d) methanol, and (g) water using 225-nm pump and 260-nm probe pulses. [(b), (e), and (h)] The time-energy maps retrieved from (a), (d), and (g), respectively. [(c), (f), and (i)] Time evolution of average eBE obtained from (a), (d), and (g) (black) and (b), (e), and (h) (red), respectively. Adapted with permission from Nishitani *et al.*, Sci. Adv. **5**, eaaw6896 (2019). Copyright 2019 Author(s), licensed under a Creative Commons Attribution 4.0 (CC-BY) license.

Nishitani *et al.* performed accurate measurements of the eBE distribution of e_{aq}^{-} and examined the validity of the analysis by Luckhaus *et al.*[60] They employed ultrafast photoelectron spectroscopy of liquids with EUV probe pulses ($h\nu$ = 27.9 eV) generated using HHG with a 400-nm driving laser and spectral purification using a time-preserving grating monochromator.[132] Figure 7 shows their experimental result along with the least squares fit and the prediction by Luckhaus *et al.* The least squares fit corresponds to an almost perfect Gaussian centered at 3.76 ± 0.05 eV with a FWHM of 1.02 ± 0.04 eV; the predicted shoulder[60] was absent. The eBE spectra of solvated electrons in methanol and ethanol were similarly measured, and their VBE values were determined to be 3.35 and 3.21 eV, respectively.[132]

EUV photoelectron spectroscopy produces high PKEs, at which the influence of inelastic scattering can safely be minimized; however, its short probing depth results in extremely low signal levels, and the experimental complexity of an EUV laser hinders wide application to solution chemistry. Ultrafast UV photoelectron spectroscopy of liquids is advantageous for a considerably higher signal intensity and less demanding implementation. The problem, however, was its susceptibility to inelastic scattering effects in liquid. In order to solve this problem, we developed a method for retrieving the initial kinetic energy distribution created in the conduction band—prior to inelastic scattering—from the PKE distribution experimentally measured.[132]

For this retrieval, we utilized an accurately determined eBE distribution of solvated electrons. The eBE distribution enable us to predict the initial electron kinetic energy distribution, $G_{\hbar\omega}(E)$, where E is measured from the vacuum level, created in the conduction band by excitation of solvated electrons with photon energy ($\hbar\omega$). On the other hand, the actual PKE distribution, $g_{\hbar\omega}(E)$, has already been measured.[131] A number of $G_{\hbar\omega}(E)$–$g_{\hbar\omega}(E)$ pairs determined at various $\hbar\omega$ values provide a $G_{\hbar\omega}(E) \rightarrow g_{\hbar\omega}(E)$ linear mapping due to inelastic scattering. [If no inelastic scattering occurs, $G_{\hbar\omega}(E) = g_{\hbar\omega}(E)$.] The inverse mapping $g_{\hbar\omega}(E) \rightarrow G_{\hbar\omega}(E)$ allows us to retrieve the kinetic energy distribution prior to inelastic scattering from a given PKE distribution. In an actual analysis, an experimental PKE time-energy map, $I_{PKE}(E, t)$, is expanded with a set of $g_i(E)$ and their time-dependent coefficients, $c_i(t)$, as $I_{PKE}(E,t) = \sum_i c_i(t) g_i(E)$, where i indicates discrete photon energies. Then, a true time-energy map, $I_{eKE}(E,t)$, is obtained by replacing $g_i(E)$ with a corresponding Gaussian-shaped kinetic energy distribution, $G_j(E)$, as $I_{eKE}(E,t) = \sum_i c_i(t) G_j(E)$.[132]

Figure 8 compares the experimental PKE maps measured for CTTS reactions from I^{-} to ethanol, methanol, and water[133] with their retrieved time-energy maps.[132] Here, 225-nm pump pulses promote a valence electron of I^{-} to a metastable excited state, from which adiabatic electron transfer occurs in solvent. The solvation shell surrounding I^{-} responds to photodetachment and stabilizes the electron by solvent reorganization. The time-evolution of eBE measured using time-delayed 260-nm probe pulses indicates the time scale of this energy stabilization. As spectral blurring and energy-shift due to inelastic scattering were corrected, the retrieved spectra exhibited much narrower spectral widths and upshifted kinetic energy (down-shifted eBE). Figures 8(c), 8(f), and 8(i) compare the average eBEs calculated from the original and retrieved time-energy maps, which reveal that the time constants are essentially the same, while the eBEs differ by as much as 1 eV. The difference between the raw and retrieved data diminishes in the order of ethanol, methanol, and water because the inelastic scattering effect

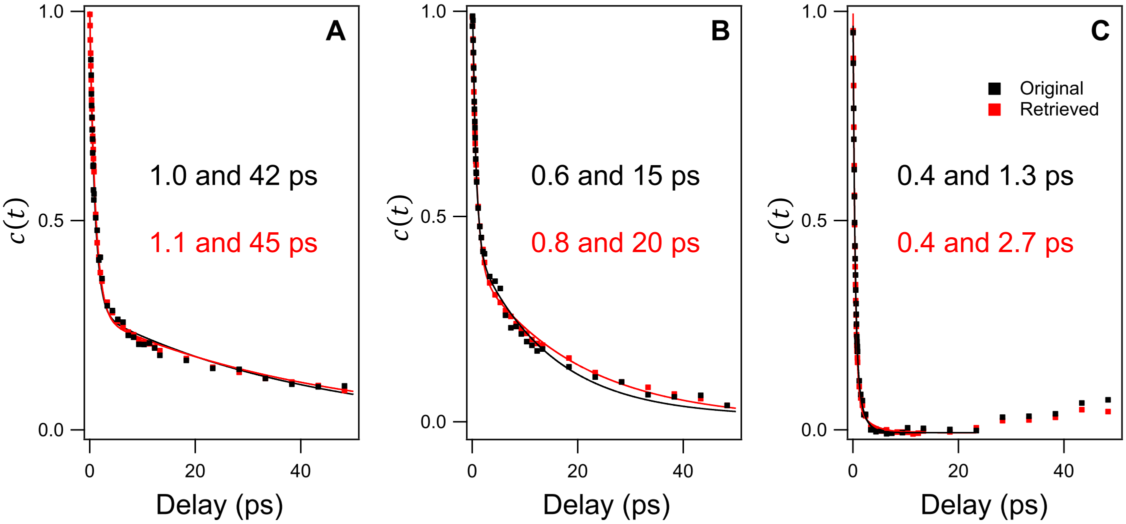

FIG. 9. Time-correlation function *c*(*t*) determined from the ultrafast UV photoelectron spectra of the CTTS reaction from I^{-} to (a) ethanol, (b) methanol, and (c) water. The original (black) and retrieved (red) data points are shown. Time constants and simulated curves in solid lines were obtained by the least squares fitting. In (c), an unexpected increase of *c*(*t*) by less than 0.1 is seen after 25 ps, which was excluded from the least squares fitting. Reproduced with permission from Nishitani *et al.*, Sci. Adv. **5**, eaaw6896 (2019). Copyright 2019 Author(s), licensed under a Creative Commons Attribution 4.0 (CC-BY) license.

diminishes for smaller kinetic energy (or higher VBE). Comparison of the three solvents clearly reveals that the solvent response of liquid water is considerably faster than those of alcohols. The results shown in Figs. 8(c), 8(f), and 8(i) can be readily transformed into a time-correlation function $c(t)$, which is a standard representation in theoretical and experimental studies on solvation dynamics, as shown in Fig. 9. The solvation times are in reasonable agreement with the literature values. Ultrafast librational responses of these solvents, expected to be within 30 fs, are not identified here because solvated electrons are produced by CTTS reactions with finite reaction times.

Ultrafast internal conversion of e_{aq}^{-}[46] from the excited to the ground electronic state received much debate among experimentalists and theorists for many years.[134–141] Barbara, Wiersma, and their co-workers reported detailed studies using transient absorption spectroscopy, and adiabatic and nonadiabatic relaxation models were debated.[46,134,135,137] The former assumes that an adiabatic solvation in the excited state precedes internal conversion. The latter suggests that ultrafast internal conversion in ∼50 fs occurs prior to the completion of solvation in the excited state. Neumark and co-workers performed ultrafast photoelectron spectroscopy of e_{aq}^{-} with 800-nm pump and 266-nm probe pulses and reported an excited-state decay constant of 75 ± 12 fs and the ground-state bleach recovery in 400 ± 70 fs.[142] As described in Sec. IV B in this review, Karashima *et al.* applied angle-resolved photoelectron spectroscopy[143] to this problem, and they obtained time constants of 60 ± 10 fs for the internal conversion and 520 ± 30 fs for the subsequent relaxation of the hot ground state. Thus, all photoelectron spectroscopic studies supported the nonadiabatic dynamics model. It is interesting

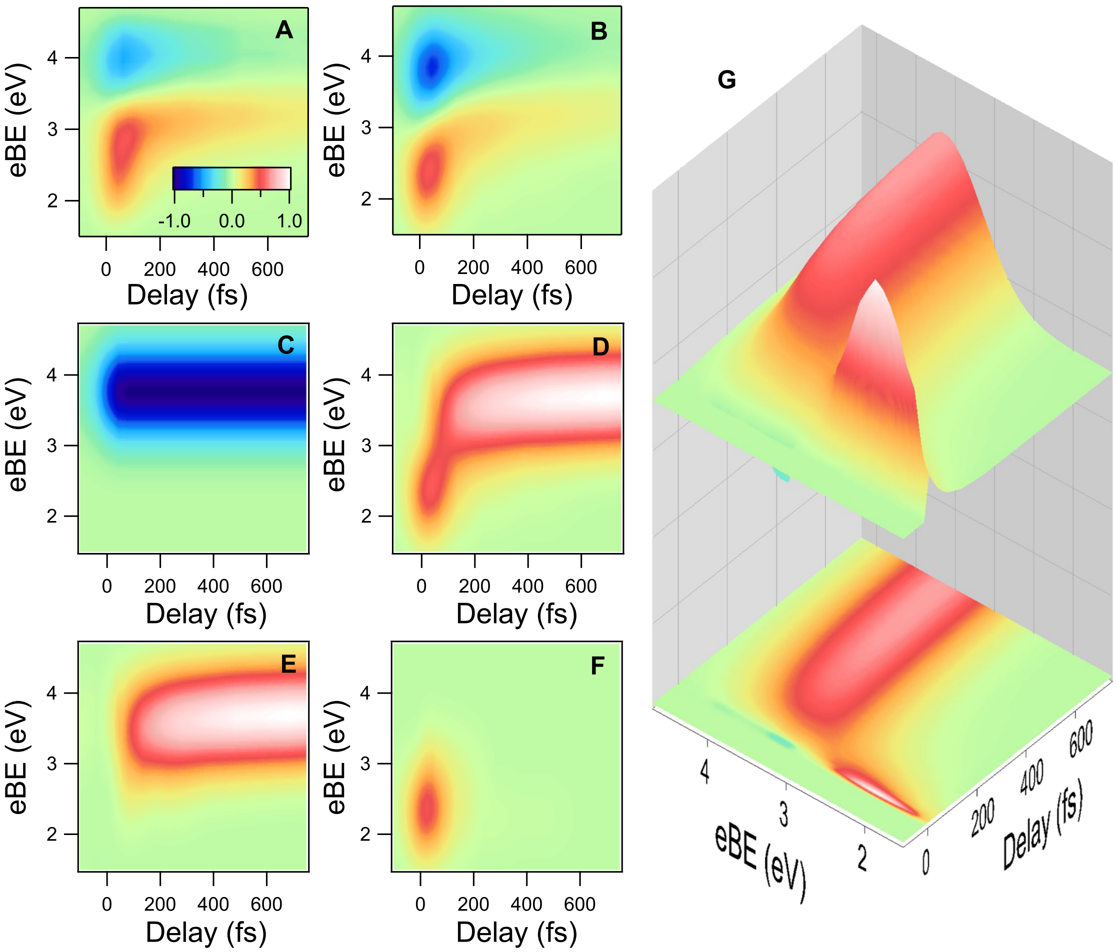

FIG. 10. (a) eBE time-energy map measured for ultrafast internal conversion of e_{aq}^{-} with the 720-nm pump and 270-nm probe pulses. (b) Retrieved eBE time-energy map. (c) Negative signal component calculated from the photoelectron spectrum separately measured for e_{aq}^{-} at thermal equilibrium. (d) Positive signal component of the distribution calculated from (b) and (c). (e) Signal from the ground state in (d). (f) Signal from the excited state in (d). (g) Prediction of photoelectron spectra obtained with 5-fs time-resolution. Adapted with permission from Nishitani *et al.*, Sci. Adv. **5**, eaaw6896 (2019). Copyright 2019 Author(s), licensed under a Creative Commons Attribution 4.0 (CC-BY) License.

to see how the newly developed retrieval method assists with unambiguous analysis of ultrafast UV photoelectron spectroscopy of e_{aq}^-.

Figure 10(a) shows the observed eBE time-energy map, prior to the spectral retrieval, for 720-nm excitation of hydrated electrons in a microjet and 270-nm photoemission.[132] The signal-to-noise level is considerably higher than that in previous studies. Application of the retrieval method provides Fig. 10(b), in which red corresponds to enhanced photoemission, while blue corresponds to the ground state bleach and its recovery. By subtracting the ground-state bleach signal [Fig. 10(c)] calculated from the photoelectron spectrum of e_{aq}^- at thermal equilibrium, the genuine pump-probe enhanced signal is obtained as shown in Fig. 10(d), which can be separated into the photoemission signal from the ground state [Fig. 10(e)] and the excited state [Fig. 10(f)]. From Fig. 10(f), the excited-state lifetime was determined to be 64 fs. The ground state signal provided two solvation times of ~230 and 910 fs, which are in good agreement with those previously suggested for liquid water.[144–146] Figure 10(g) shows the time-energy map expected for measurements with the time-resolution of 5 fs.[132]

B. Time and angle-resolved photoelectron spectroscopy

PKE is the primary observable in photoelectron spectroscopy, while photoelectron angular anisotropy is another equally important observable. However, since the elastic scattering cross section of an electron is quite large in the low PKE region, angular anisotropy is not often observed with UV photoelectron spectroscopy of liquids. As an exceptional example, Yamamoto *et al.* reported ultrafast time- and angle-resolved photoelectron spectroscopy of the CTTS reaction in aqueous DABCO (1,4-diazabicyclo[2,2,2]octane) solution.[147] They excited a microjet of the DABCO solution with 226-nm pump pulses and observed photoemission induced by time-delayed 260-nm probe pulses with varying polarization directions using a linear TOF spectrometer [Fig. 11(a)]. Figure 11(b) presents the observed photoelectron spectra; the eBE distribution is initially peaked at around 2.5 eV, and it shifts to 3.4 eV. This change in eBE is due to electron transfer from DABCO to bulk water. The excited states of DABCO accessible with the 226-nm pump pulses are the 3*s* and 3*p* Rydberg states. Their Rydberg characters are maintained in hydrated DABCO, while the Rydberg electron density penetrates unoccupied molecular orbitals of water. Quantum Mechanics/Molecular Mechanics (QM/MM) calculations indicated that photoexcitation to the 3*p* state of DABCO is followed by internal conversion to the 3*s* state, from which an electron is transferred to liquid water. The results of angle-resolved measurements are shown in Fig. 12. At 100 fs, when the excitation is still localized in DABCO, the photoemission is anisotropic with the maximum flux along the probe laser polarization direction. On the other hand, the photoemission becomes isotropic after an electron is transferred to bulk water and thermalizes. The lower panels in Fig. 12 show the anisotropic component extracted from the data shown in the upper panel; a narrow anisotropic kinetic energy distribution is ascribed to the Rydberg state of DABCO. The clear photoelectron angular anisotropy from DABCO is ascribed to the surface activity of this molecule. DABCO is hydrophobic due to its three aliphatic bridges [see its molecular structure in Fig. 11(b)] and is segregated on the liquid water surface, which has been experimentally confirmed from N(1s) XPS of an aqueous DABCO solution.[147] The CTTS reaction from DABCO to liquid water is completed within a picosecond, and photoemission at 3 ps occurs from the ground state of e_{aq}^-. The isotropic photoemission from e_{aq}^- indicates that it is created in bulk liquid water under the segregated DABCO molecule and elastic scattering of a photoelectron eliminates photoelectron anisotropy.

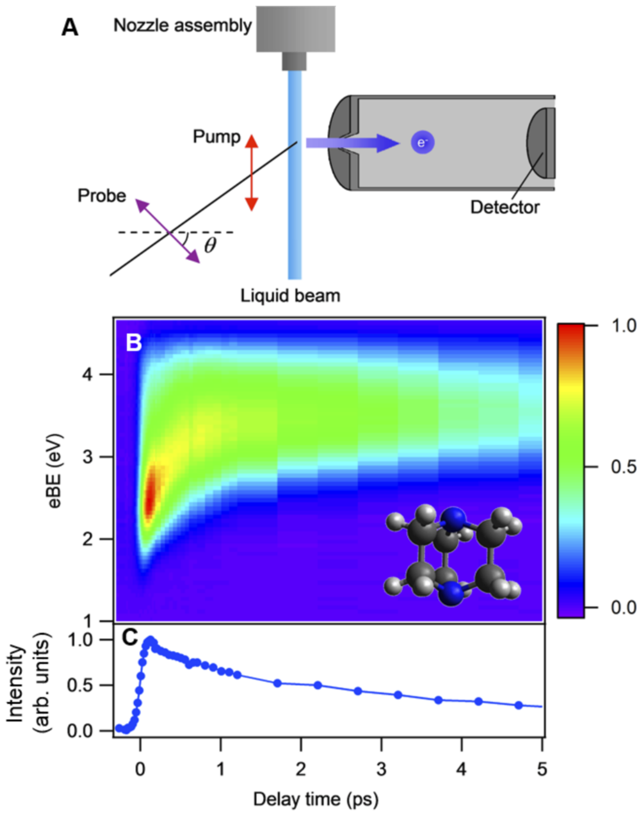

FIG. 11. (a) Schematic diagram of time- and angle-resolved photoelectron spectroscopy. (b) Two-dimensional false color map of photoelectron spectra measured for aqueous 0.1 mol/l DABCO solutions at different pump-probe time delays. The pump and probe laser wavelengths were 226 and 260 nm, respectively. (c) Total electron intensity profile obtained from (b) by integrating the distribution at each delay time over eBE. Adapted with permission from Yamamoto *et al.*, Phys. Rev. Lett. **112**, 187603 (2014). Copyright 2014 American Physical Society.

As mentioned earlier, ultrafast internal conversion of e_{aq}^- [46] from the excited to the ground electronic state has been the benchmark system in studies of ultrafast nonadiabatic dynamics in aqueous solution. One of the keys for its elucidation was spectroscopic differentiation of the excited and ground state of e_{aq}^- during the course of internal conversion. Karashima *et al.*[143] attacked this problem using time and angle-resolved photoelectron spectroscopy. Figure 13(A) shows the experimental geometry; the ω_1 pulse (200 nm) generates e_{aq}^- via CTTS from Br^- to bulk water, and the ω_2 pulse (700 nm) promotes e_{aq}^- to the excited state. Finally, the ω_3 pulse (350 nm) induces

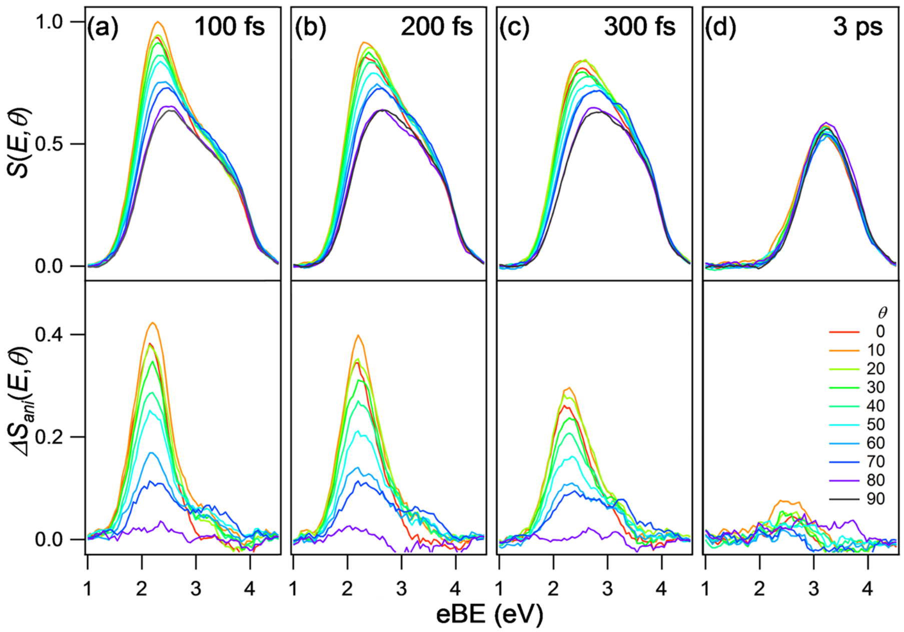

FIG. 12. Photoelectron spectra of aqueous 0.5 mol/l DABCO solution as a function of the polarization angle of the probe pulse θ with respect to the electron detection axis. The spectra were observed at different pump-probe time delays of (a) 100 fs, (b) 200 fs, (c) 300 fs, and (d) 3 ps. Reproduced with permission from Yamamoto *et al.*, Phys. Rev. Lett. **112**, 187603 (2014). Copyright 2014 American Physical Society.

photoemission. The photoelectron spectra of e^-_{aq} measured at different ω_2–ω_3 delay times and different ω_3 pulse polarization angles (θ_3) are shown in Fig. 13(B). Anisotropy is observed for short delay times, while it vanishes at 400 fs when the excited state is already depopulated. The analysis indicates that the photoemission anisotropy parameter of the excited state is 0.16 and that of the ground state is 0; the internal conversion time constant was estimated to be 60 ± 10 fs. It is noted that the first excited state of e^-_{aq} is triply degenerate, and linearly polarized pump pulses preferentially excite one of them to create electron orbital alignment. The photoemission anisotropy in Fig. 13 at the time origin varies with the pump pulse polarization, while the polarization dependence vanishes after 40 fs. The results suggest that the electron orbital alignment is lost within 40 fs due to nonadiabatic transitions among the degenerate excited states.

C. Pump-probe experiments on redox reactions

Chergui, Aziz, and their co-workers applied ultrafast photoelectron spectroscopy using high harmonics to photoinduced redox reactions of inorganic complexes.[43,148] The inset in Fig. 14 shows the static photoelectron spectra of aqueous $K_4[Fe(CN)_6]$ and $K_3[Fe(CN)_6]$ solutions, which reveal well-separated HOMO bands for different oxidation states of Fe. The main panel of Fig. 14 shows transient photoelectron spectra measured for $[Fe(CN)_6]^{3-}$ at various pump-probe delay times between the 395-nm pump pulses and 39-eV probe pulses; note that the vertical axis is logarithmic to display a very weak transient signal. The spectral region of the HOMO exhibits a clear response to the ligand-to-metal charge-transfer (LMCT) process. The integrated photoelectron counts between 5.7 and 6.5 eV are shown in the main panel of Fig. 15. At the time origin, a strong coherence artifact representing the cross-correlation of the laser pulses appears,[149] which is followed by population decay of Fe^{2+} with a time constant of 470 ± 130 fs. The inset in Fig. 15 is a similar plot of the integrated signal over 7.15–7.85 eV, which shows only the coherence artifact.[149] As seen here, a major challenge in ultrafast EUV photoelectron spectroscopy of liquids is to observe a solute signal that is orders of magnitude smaller than that for the solvent. As for observing the oxidation state of transition metals, an alternative approach would be ultrafast X-ray absorption spectroscopy.

D. Computational simulation of photoelectron spectra

As far as we have noticed, the only theoretical simulation of ultrafast photoelectron spectroscopy of liquids thus far has been the work of Schwartz and co-workers on internal conversion of e^-_{aq}.[150] The purpose of their simulation was to differentiate cavity and noncavity models of e^-_{aq}. Molecular orbital and density functional theory (DFT) calculations of e^-_{aq} suggest that e^-_{aq} is in a cavity state, in which a bubble-like electron cloud is electrostatically stabilized by 4–6 water molecules in the first hydration shell with the OH bond pointing toward the center of the cloud.[151–154] Computational simulations using a pseudopotential[155–157] by Turi and Borgis also suggested the cavity state.[158] Schwartz challenged this conventional picture and proposed an alternative one based on calculations using their own new pseudopotential between an electron and a water molecule;[157] Schwartz suggested that water molecules are more densely packed in an electron cloud.[157] Zho and Schwartz simulated time-resolved photoelectron spectra using the noncavity and cavity forming pseudopotentials and showed that the noncavity model provides better agreement with the photoelectron spectra.[150]

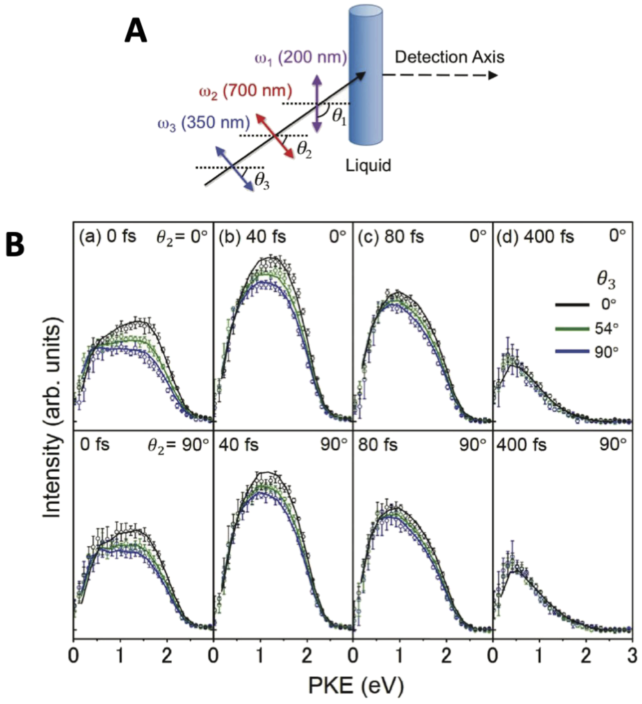

FIG. 13. (A) Experimental geometry, in which θ_1 is 90°. (B) Photoelectron kinetic energy distributions observed for e^-_{aq} in H_2O for Δt_{23} values of (a) 0, (b) 40, (c) 80, and (d) 400 fs. θ_2 is 0° and 90° for the upper and lower panels, respectively. The black, green, and blue colors correspond to θ_3 of 0°, 54°, and 90°, respectively. The dots and error bars represent the experimental data and their standard deviation, while the solid lines are simulations using the decay associated spectra and the anisotropy parameter (β_2) assumed for the τ_1 component. The anisotropy parameter of the τ_2 component was assumed to be zero. The cross-correlation time between ω_2 and ω_3 was 55 fs. Reproduced with permission from Karashima *et al.*, Phys. Rev. Lett. **116**, 137601 (2016). Copyright 2016 American Physical Society.

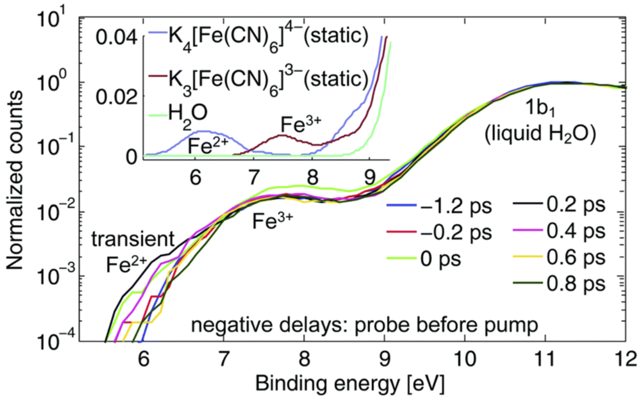

FIG. 14. Time-resolved photoelectron spectra of aqueous ferricyanide upon photoexcitation of the LMCT band centered at ∼420 nm. The inset shows the static (unpumped) photoelectron spectra of water and aqueous ferro- and ferricyanide solutions in the region of the $Fe^{2+/3+}$ HOMO. Reproduced with permission from Ojeda *et al.*, Phys. Chem. Chem. Phys. **19**, 17052 (2017). Copyright 2017 PCCP Owner Societies.

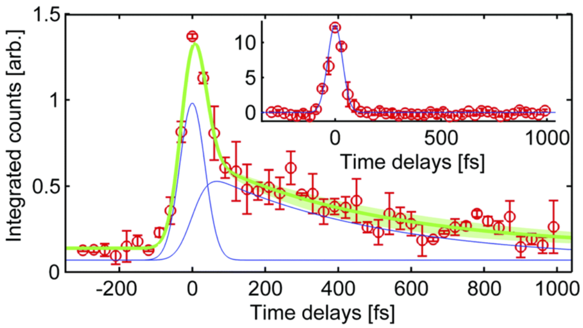

FIG. 15. Integrated raw photoelectron counts from photoelectron spectra (red circles) normalized to the intensity of the water HOMO band. Inset: in a binding energy window (7.15–7.85 eV) corresponding to the Fe^{3+} HOMO of the unpumped molecules, where the cross-correlation signal is evident. Main figure: in a BE window (5.7–6.5 eV) containing the Fe^{2+} transient signal, which decays with a time constant of 475 ± 130 fs. Error bars represent the standard deviation over several experimental runs. Reproduced with permission from Ojeda *et al.*, Phys. Chem. Chem. Phys. **19**, 17052 (2017). Copyright 2017 PCCP Owner Societies.

As for one-photon photoelectron spectroscopy of liquids, the VBEs of simple ions and organic molecules were theoretically analyzed using various solvation models, such as a polarizable continuum or explicit inclusion of discrete water molecules with their snapshots from molecular dynamics simulations.[159,160] For example, Slavíček *et al.* have simulated the photoelectron spectra of cytidine and deoxythymidine in aqueous solutions using a nonequilibrium polarizable continuum model.[161] Their calculations well reproduced the VBEs and indicated that electrostatic screening by hydration makes the VBE insensitive to sugar and phosphate. Krylov and co-workers calculated the lowest binding energies of phenol (7.9 eV) and phenolate (7.7 eV) using the equation-of-motion ionization potential coupled-cluster (EOM-IP-CCSD) method and an effective fragment potential for solvation structure calculated using molecular dynamics, which provided fair agreement with the experimental values of 7.8 ± 0.1 and 7.1 ± 0.1 eV.[162] A similar study was undertaken by Tentscher *et al.*, who predicted the two lowest eBEs of aniline, imidazole, veratrole alcohol, and phenol using EOM-IP-CCSD.[163]

The photoelectron spectrum of liquid water has been computed using several methods. Slavíček and co-workers considered water clusters as a model for liquid water and applied the reflection principle and Koopmans' theorem;[161] the nuclear density was calculated using a path-integral-based molecular dynamics simulation, and the eBE was obtained using density functional theory (DFT) with optimally tuned range-separated hybrid (RSH) functionals. The range-separation parameter of the functional was individually optimized for different cluster sizes, but the parameter converged for large clusters ($N > 30$). Since the method does not provide relative ionization cross sections, they were calibrated using experimental data. Figure 16 compares the theoretical and experimental spectra. The theoretical eBEs for the outer valence orbitals are too low by 0.2–0.4 eV due to insufficient long-range polarization in a finite-sized cluster and insufficient accuracy in the electronic structure calculations. The experimental $2a_1$ band exhibits

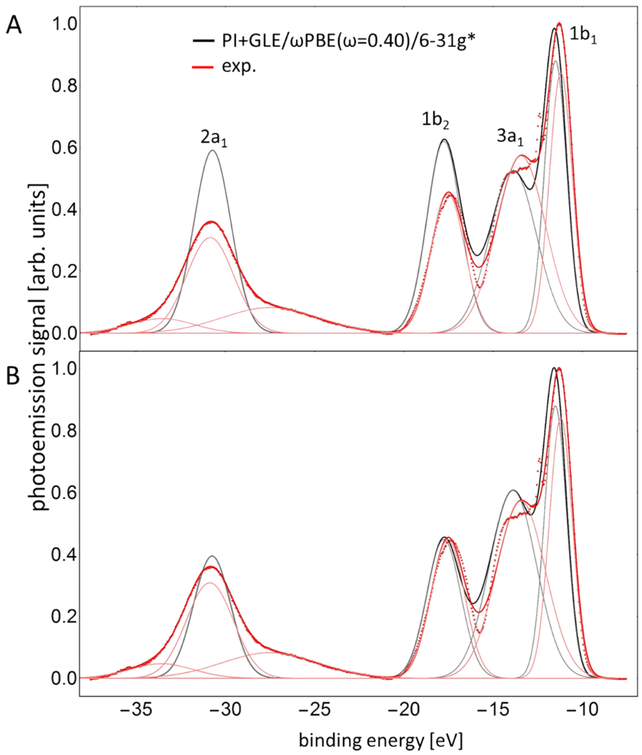

FIG. 16. (a) Comparison of photoelectron spectra calculated for $(H_2O)_{100}$ clusters (black curve) and experimental result for bulk water (red dots). The fit to the experimental data is depicted as a red curve. Theoretical curves are fitted with four Gaussian functions in thin gray lines. The least squares fit to the experimental data, shown in thin red lines, includes additional Gaussian functions to express broad peaks on both sides of the $2a_1$ peak, which cannot be calculated using the single-particle picture of the $(2a_1)^{-1}$ cationic state. (b) Theoretical spectrum weighted with experimental photoionization cross sections. The spectrum was normalized so that the surface below the experimental and theoretical curves is equal. The experimental curves were measured at 200 eV, and the backgrounds due to scattered electrons were carefully subtracted. Reproduced with permission from Hollas *et al.*, J. Chem. Theory Comput. **12**, 5009 (2016). Copyright (2016) American Chemical Society.

satellite peaks on both sides due to electron correlation, while this feature is not obtained in the theoretical model with one-electron approximation. Galli and co-workers benchmarked DFT and many-body perturbation theory (MBPT) at the G_0W_0 level with different exchange-correlation functionals.[164,165] Figure 17 compares theoretical spectra calculated for an aqueous 0.87 mol/l NO_3^- solution using DFT with different functionals; the computations were performed using cubic cells containing one anion and 63 water molecules with a positive diffuse background charge to maintain the charge balance in the cell.[165] The band positions computed using DFT with a RSH or self-consistent hybrid (sc-hybrid) functional agree rather well with the experiment. Many-body perturbation theory at the G_0W_0 level was superior to DFT in terms of accuracy, while the improvement was relatively small with TSH and sc-hybrid functionals because they were already rather accurate with DFT. The approach using optimally tuned RSH was also discussed in a recent review.[166]

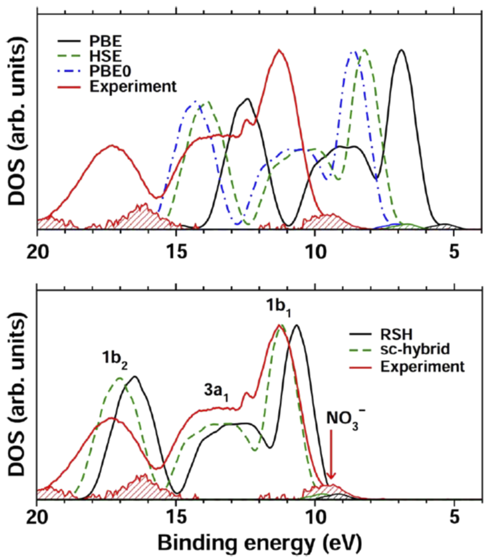

FIG. 17. Experimental and theoretical photoelectron spectra of $NaNO_3$ solution. The experimental spectrum is shown as the solid red line. The theoretical results were obtained with DFT using several functionals: the Perdew-Burke-Ernzerhof (PBE) exchange-correlation functional, the Heyd-Scuseria-Ernzerhof (HSE) functional, and PBE0 (top panel), as well as RSH and sc-hybrid functionals (bottom panel). The shaded areas represent the differential valence photoelectron spectra obtained by subtracting the water spectrum from the raw experimental $NaNO_3$ spectrum, and the theoretical density of state (DOS) contributions from the NO_3^- HOMO. All energy levels are relative to vacuum. Experimental and theoretical DOS intensities were rescaled with respect to the $1b_1$ peak of water at 11.31 eV. The differential spectra and theoretical HOMO DOS intensity were magnified (3×) for clarity. Reproduced with permission from Pham *et al.*, Sci. Adv. **3**, e1603210 (2017). Copyright 2017 Author(s), licensed under a Creative Commons Attribution 4.0 (CC-BY) License.

V. CONCLUSION AND OUTLOOK

Ultrafast photoelectron spectroscopy of liquids enables direct access to electron binding energies of transient states/species, and it provides deeper insights into electron transfer, redox, and nonadiabatic dynamics in aqueous solutions. It was not initially clear whether the photoelectron spectroscopy of liquids provides specific information about the interface or more general information about the bulk because the inelastic mean free path and effective attenuation length of an electron in liquid water had not been established. However, experiments indicate that the effective attenuation length of an electron flux in liquid water is several nm in the kinetic energy region less than 20 eV, and this is sufficiently large for photoelectron spectroscopy to probe the bulk properties of aqueous solutions with large dielectric constants. The dynamical constants extracted by photoelectron spectroscopy are in excellent agreement with those obtained by transient absorption spectroscopy for bulk solution. While transient absorption spectroscopy is extremely useful and even applicable to biological samples under a microscope, the interpretation of the results can be rather complex. A good example was the excited-state dynamics of hydrated electrons, for which overlapping photoabsorption/emission contributions and a rapid spectral shift made the analysis highly complex. Ultrafast photoelectron spectroscopy of liquids clarified the ultrafast nonadiabatic dynamics of hydrated electrons. The internal conversion time was determined to be 60 fs, which contradicts with theory. There are no computational simulations sufficiently accurate to predict electron scattering in liquid water below 100 eV, whereas experimental studies have been few and far between. Elucidation of electron scattering in liquid water is essential for radiation chemistry and biology, and further improvement is indispensable for simulations as well as experiments.

Ultrafast photoelectron spectroscopy using UV pulses is free from strong photoionization of solvents, which is an advantage over EUV spectroscopy for observing the excited-state dynamics of a solute. On the other hand, UV photoelectron spectra exhibit energy shifts and broadening owing to the inelastic scattering of the electrons. The spectral retrieval method we demonstrated seems highly useful for analysis, and further improvements and applications should be pursued. One caution for it is that the g-G transformation must be determined using a chemical species with a similar depth profile with that of a target species.

Photoelectron spectroscopy of liquids should be applicable to the real-time observation of interfacial electron transfer and redox reactions using solutions containing nanoparticles. There is strong demand for elucidating the electron transfer dynamics between solids and liquids to solve practical problems such as solar energy conversion, energy storage, and others. Theoretical simulations of electronic dynamics in aqueous solution will become more accurate in the near future, and a valuable interplay between theory and experiment is anticipated.

ACKNOWLEDGMENTS

This research was supported by JSPS KAKENHI (Grant No. 15H05753). The author thanks Yo-ichi Yamamoto, Junichi Nishitani, Shutaro Karashima, and Christopher W. West for their contributions to ultrafast photoelectron spectroscopy of liquids at Kyoto University. Contributions by Ying Tang and Yoshi-Ichi Suzuki in the initial efforts of this project are also gratefully appreciated.

REFERENCES

[1] R. E. Smalley *et al.*, J. Chem. Phys. **61**, 4363 (1974).
[2] H. W. Kroto *et al.*, Nature **318**, 162 (1985).
[3] A. H. Zewail, Angew. Chem., Int. Ed. **39**, 2586 (2000).
[4] J. B. Kim *et al.*, Science **349**, 510 (2015).
[5] R. T. Skodje *et al.*, Phys. Rev. Lett. **85**, 1206 (2000).
[6] M. H. Qiu *et al.*, Science **311**, 1440 (2006).
[7] K. Liu, Adv. Chem. Phys. **149**, 1 (2012).
[8] F. Krausz and M. Ivanov, Rev. Mod. Phys. **81**, 163 (2009).
[9] S. Y. T. Van De Meerakker *et al.*, Nat. Phys. **4**, 595 (2008).
[10] Y. Shao *et al.*, Phys. Chem. Chem. Phys. **8**, 3172 (2006).
[11] A. Krylov *et al.*, J. Chem. Phys. **149**, 180901 (2018).
[12] M. Ben-Nun and T. J. Martinez, Adv. Chem. Phys. **121**, 439 (2002).
[13] B. R. Brooks *et al.*, J. Comput. Chem. **30**, 1545 (2009).
[14] I. S. Ufimtsev and T. J. Martinez, J. Chem. Theory Comput. **5**, 2619 (2009).
[15] P. Ball, Chem. Rev. **108**, 74 (2008).
[16] P. Wernet *et al.*, Science **304**, 995 (2004).
[17] A. Nilsson and L. G. M. Pettersson, Chem. Phys. **389**, 1 (2011).
[18] S. Hufner, *Photoelectron Spectroscopy: Principles and Applications* (Springer-Verlag, 2003).
[19] K. Siegbahn, Rev. Mod. Phys. **54**, 709 (1982).
[20] D. W. Turner, Philos. Trans. R. Soc., A **268**, 7 (1970).
[21] D. W. Turner and M. I. Aljobory, J. Chem. Phys. **37**, 3007 (1962).
[22] F. I. Vilesov *et al.*, Dokl. Akad. Nauk SSSR **138**, 1329 (1961).
[23] P. Delahay, Acc. Chem. Res. **15**, 40 (1982).
[24] H. Siegbahn, J. Phys. Chem. **89**, 897 (1985).
[25] B. Baron *et al.*, J. Chem. Phys. **51**, 2562 (1969).
[26] I. Watanabe *et al.*, J. Chem. Phys. **73**, 2057 (1980).
[27] M. Faubel, in *Photoionization and Photodetachment*, edited by C.-Y. Ng (World Scientific, Singapore, 2000), Vol. 1.
[28] F. Eschen *et al.*, J. Phys.: Condens. Matter **7**, 1961 (1995).
[29] H. Siegbahn and K. Siegbahn, J. Electron Spectrosc. Relat. Phenom. **2**, 319 (1973).
[30] M. Faubel *et al.*, Z. Phys. D: At., Mol. Clusters **10**, 269 (1988).
[31] K. R. Wilson *et al.*, Rev. Sci. Instrum. **75**, 725 (2004).
[32] M. Faubel *et al.*, J. Chem. Phys. **106**, 9013 (1997).
[33] J. Y. Kohno *et al.*, J. Phys. Chem. A **104**, 243 (2000).
[34] F. Mafune *et al.*, Chem. Phys. Lett. **199**, 615 (1992).
[35] T. Kondow and F. Mafune, Annu. Rev. Phys. Chem. **51**, 731 (2000).
[36] B. Winter and M. Faubel, Chem. Rev. **106**, 1176 (2006).
[37] K. R. Siefermann *et al.*, Nat. Chem. **2**, 274 (2010).
[38] Y. Tang *et al.*, Phys. Chem. Chem. Phys. **12**, 3653 (2010).
[39] A. Lubcke *et al.*, Phys. Chem. Chem. Phys. **12**, 14629 (2010).
[40] M. H. Elkins *et al.*, Science **342**, 1496 (2013).
[41] I. Jordan *et al.*, Rev. Sci. Instrum. **86**, 123905 (2015).
[42] J. Ojeda *et al.*, Struct. Dyn. **3**, 023602 (2016).
[43] N. Engel *et al.*, Phys. Chem. Chem. Phys. **19**, 14248 (2017).
[44] J. W. Riley *et al.*, J. Phys. Chem. Lett. **9**, 678 (2018).
[45] G. Kumar *et al.*, Faraday Discuss. **212**, 359 (2018).
[46] L. Turi and P. J. Rossky, Chem. Rev. **112**, 5641 (2012).
[47] E. J. Hart and J. W. Boag, J. Am. Chem. Soc. **84**, 4090 (1962).
[48] E. Alizadeh and L. Sanche, Chem. Rev. **112**, 5578 (2012).
[49] J. V. Coe *et al.*, J. Chem. Phys. **92**, 3980 (1990).
[50] J. V. Coe, Int. Rev. Phys. Chem. **20**, 33 (2001).
[51] J. V. Coe *et al.*, Int. Rev. Phys. Chem. **27**, 27 (2008).
[52] R. M. Young and D. M. Neumark, Chem. Rev. **112**, 5553 (2012).
[53] J. R. R. Verlet *et al.*, Science **307**, 93 (2005).
[54] L. Turi *et al.*, Science **310**, 1769 (2005).
[55] L. Turi *et al.*, Science **309**, 914 (2005).
[56] A. T. Shreve *et al.*, Chem. Phys. Lett. **493**, 216 (2010).
[57] J. A. Kloepfer *et al.*, J. Chem. Phys. **117**, 766 (2002).
[58] X. Y. Chen and S. E. Bradforth, Annu. Rev. Phys. Chem. **59**, 203 (2008).
[59] K. Nishizawa *et al.*, J. Chin. Chem. Soc. **60**, 1403 (2013).
[60] D. Luckhaus *et al.*, Sci. Adv. **3**, e1603224 (2017).
[61] P. Kruit and F. H. Read, J. Phys. E: Sci. Instrum. **16**, 313 (1983).
[62] T. Fuji, T. Horio, and T. Suzuki, Opt. Lett. **32**, 2481 (2007).
[63] T. Horio *et al.*, Opt. Express **21**, 22423 (2013).
[64] T. Horio *et al.*, Opt. Lett. **39**, 6021 (2014).
[65] P. B. Corkum, Phys. Rev. Lett. **71**, 1994 (1993).
[66] M. Lewenstein *et al.*, Phys. Rev. A **49**, 2117 (1994).
[67] M. Salmeron and R. Schlogl, Surf. Sci. Rep. **63**, 169 (2008).
[68] H. Tissot *et al.*, Top. Catal. **59**, 605 (2016).
[69] R. Seidel *et al.*, Rev. Sci. Instrum. **88**, 073107 (2017).
[70] L. Artiglia *et al.*, Nat. Commun. **8**, 700 (2017).
[71] E. A. Seddon *et al.*, Rep. Prog. Phys. **80**, 115901 (2017).
[72] L. Poletto *et al.*, Rev. Sci. Instrum. **80**, 123109 (2009).
[73] F. Frassetto *et al.*, Opt. Express **19**, 19169 (2011).
[74] J. Nishitani *et al.*, Struct. Dyn. **4**, 044014 (2017).
[75] J. Metje *et al.*, Opt. Express **22**, 10747 (2014).
[76] C. Corder *et al.*, Struct. Dyn. **5**, 054301 (2018).
[77] S. Hadrich *et al.*, Nat. Photonics **8**, 779 (2014).

[78] J. Rothhardt *et al.*, Opt. Express **24**, 18133 (2016).

[79] F. Emaury *et al.*, Optica **2**, 980 (2015).

[80] F. Labaye *et al.*, Opt. Lett. **42**, 5170 (2017).

[81] H. Wang *et al.*, Nat. Commun. **6**, 7459 (2015).

[82] C. Marceau *et al.*, J. Phys. Commun. **1**, 015009 (2017).

[83] D. Popmintchev *et al.*, Science **350**, 1225 (2015).

[84] T. T. Luu *et al.*, Nature **521**, 498 (2015).

[85] F. Langer *et al.*, Nature **533**, 225 (2016).

[86] Y. S. You *et al.*, Nat. Commun. **8**, 724 (2017).

[87] N. Yoshikawa *et al.*, Science **356**, 736 (2017).

[88] T. T. Luu and H. J. Woerner, Nat. Commun. **9**, 916 (2018).

[89] T. T. Luu *et al.*, Nat. Commun. **9**, 3723 (2018).

[90] M. Faubel and B. Steiner, Ber. Bunsengesellschaft Phys. Chem. **96**, 1167 (1992).

[91] W. L. Holstein *et al.*, J. Phys. Chem. B **103**, 3035 (1999).

[92] A. M. Duffin and R. J. Saykally, J. Phys. Chem. C **112**, 17018 (2008).

[93] N. Preissler *et al.*, J. Phys. Chem. B **117**, 2422 (2013).

[94] N. Kurahashi *et al.*, J. Chem. Phys. **140**, 174506 (2014).

[95] F. Buchner *et al.*, Phys. Chem. Chem. Phys. **15**, 11402 (2013).

[96] F. Buchner *et al.*, J. Am. Chem. Soc. **137**, 2931 (2015).

[97] H. L. Williams *et al.*, J. Chem. Phys. **148**, 194303 (2018).

[98] N. Kurahashi and T. Suzuki, Chem. Lett. **47**, 16 (2018).

[99] S. W. Ong *et al.*, Chem. Phys. Lett. **191**, 327 (1992).

[100] K. Leung *et al.*, J. Am. Chem. Soc. **131**, 18358 (2009).

[101] M. S. Azam *et al.*, J. Phys. Chem. Lett. **3**, 1269 (2012).

[102] M. S. Azam *et al.*, J. Phys. Chem. C **117**, 8840 (2013).

[103] M. S. Azam *et al.*, J. Phys.: Condens. Matter **26**, 244107 (2014).

[104] A. M. Darlington and J. M. Gibbs-Davis, J. Phys. Chem. C **119**, 16560 (2015).

[105] B. Winter *et al.*, J. Phys. Chem. A **108**, 2625 (2004).

[106] K. Nishizawa *et al.*, Phys. Chem. Chem. Phys. **13**, 413 (2011).

[107] Y. Tang *et al.*, Chem. Phys. Lett. **494**, 111 (2010).

[108] M. P. Seah and W. A. Dench, Surf. Interface Anal. **1**, 2 (1979).

[109] D. Emfietzoglou *et al.*, Nucl. Instrum. Methods Phys. Res., Sect. B **267**, 45 (2009).

[110] N. Ottosson *et al.*, J. Electron. Spectrosc. Relat. Phenom. **177**, 60 (2010).

[111] S. Thurmer *et al.*, Phys. Rev. Lett. **111**, 173005 (2013).

[112] Y. I. Suzuki *et al.*, Phys. Rev. E **90**, 010302(R) (2014).

[113] H. Shinotsuka *et al.*, Surf. Interface Anal. **49**, 238 (2017).

[114] H. T. Nguyen-Truong, J. Phys.: Condens. Matter **30**, 155101 (2018).

[115] R. Signorell *et al.*, Chem. Phys. Lett. **658**, 1 (2016).

[116] T. E. Gartmann *et al.*, Phys. Chem. Chem. Phys. **20**, 16364 (2018).

[117] S. K. Jo and J. M. White, J. Chem. Phys. **94**, 5761 (1991).

[118] R. L. Kurtz *et al.*, J. Electron Spectrosc. Relat. Phenom. **40**, 35 (1986).

[119] M. Michaud and L. Sanche, Phys. Rev. A **36**, 4684 (1987).

[120] M. Michaud *et al.*, Radiat. Res. **159**, 3 (2003).

[121] L. Nemec *et al.*, Chem. Phys. Lett. **16**, 278 (1972).

[122] L. Nemec *et al.*, J. Phys. Chem. **79**, 2935 (1975).

[123] L. Nemec *et al.*, J. Chem. Phys. **66**, 4450 (1977).

[124] A. Bernas *et al.*, Chem. Phys. **222**, 151 (1997).

[125] A. P. Gaiduk *et al.*, Nat. Commun. **9**, 247 (2018).

[126] F. Ambrosio *et al.*, J. Phys. Chem. Lett. **9**, 3212 (2018).

[127] V. Ziaei and T. Bredow, J. Phys.: Condens. Matter **30**, 215502 (2018).

[128] L. P. Oloff *et al.*, New J. Phys. **16**, 123045 (2014).

[129] R. Al-Obaidi *et al.*, New J. Phys. **17**, 093016 (2015).

[130] J. Hummert *et al.*, J. Phys. Chem. Lett. **9**, 6649 (2018).

[131] Y. Yamamoto *et al.*, J. Phys. Chem. A **120**, 1153 (2016).

[132] J. Nishitani *et al.*, Sci. Adv. **5**, eaaw6896 (2019).

[133] H. Okuyama *et al.*, J. Chem. Phys. **145**, 074502 (2016).

[134] K. Yokoyama *et al.*, J. Phys. Chem. A **102**, 6957 (1998).

[135] C. Silva *et al.*, Phys. Rev. Lett. **80**, 1086 (1998).

[136] M. F. Emde *et al.*, Phys. Rev. Lett. **80**, 4645 (1998).

[137] M. S. Pshenichnikov *et al.*, Chem. Phys. Lett. **389**, 171 (2004).

[138] M. Assel *et al.*, J. Phys. Chem. A **102**, 2256 (1998).

[139] M. Assel *et al.*, Chem. Phys. Lett. **317**, 13 (2000).

[140] A. Thaller *et al.*, Chem. Phys. Lett. **398**, 459 (2004).

[141] M. C. Cavanagh *et al.*, Chem. Phys. Lett. **396**, 359 (2004).

[142] M. H. Elkins *et al.*, J. Chem. Phys. **144**, 184503 (2016).

[143] S. Karashima *et al.*, Phys. Rev. Lett. **116**, 137601 (2016).

[144] R. Jimenez *et al.*, Nature **369**, 471 (1994).

[145] S. Roy and B. Bagchi, J. Chem. Phys. **99**, 9938 (1993).

[146] A. A. Mosyak *et al.*, J. Chem. Phys. **109**, 6390 (1998).

[147] Y. Yamamoto *et al.*, Phys. Rev. Lett. **112**, 187603 (2014).

[148] J. Ojeda *et al.*, Phys. Chem. Chem. Phys. **19**, 17052 (2017).

[149] C. A. Arrell *et al.*, Phys. Rev. Lett. **117**, 143001 (2016).

[150] C. C. Zho and B. J. Schwartz, J. Phys. Chem. B **120**, 12604 (2016).

[151] O. Marsalek *et al.*, Acc. Chem. Res. **45**, 23 (2012).

[152] F. Uhlig *et al.*, J. Phys. Chem. Lett. **3**, 3071 (2012).

[153] F. Uhlig *et al.*, J. Phys. Chem. Lett. **4**, 338 (2013).

[154] F. Uhlig *et al.*, J. Phys. Chem. A **118**, 7507 (2014).

[155] P. J. Rossky and J. Schnitker, J. Phys. Chem. **92**, 4277 (1988).

[156] J. Schnitker and P. J. Rossky, J. Chem. Phys. **131**, 037102 (2009).

[157] R. E. Larsen *et al.*, Science **329**, 65 (2010).

[158] L. Turi and D. Borgis, J. Chem. Phys. **117**, 6186 (2002).

[159] B. Winter *et al.*, J. Am. Chem. Soc. **127**, 7203 (2005).

[160] P. Slavíček *et al.*, J. Am. Chem. Soc. **131**, 6460 (2009).

[161] D. Hollas *et al.*, J. Chem. Theory Comput. **12**, 5009 (2016).

[162] D. Ghosh *et al.*, J. Phys. Chem. B **116**, 7269 (2012).

[163] P. R. Tentscher *et al.*, J. Phys. Chem. B **119**, 238 (2015).

[164] A. P. Gaiduk *et al.*, J. Am. Chem. Soc. **138**, 6912 (2016).

[165] T. A. Pham *et al.*, Sci. Adv. **3**, e1603210 (2017).

[166] E. Muchova and P. Slavíček, J. Phys.: Condens. Matter **31**, 043001 (2019).